Microwave Photonic Filter With Two Independently Tunable Passbands Using a Phase Modulator and an Equivalent Phase-Shifted Fiber Bragg Grating

Liang Gao, *Student Member, IEEE*, Jiejun Zhang, *Student Member, IEEE*, Xiangfei Chen, *Senior Member, IEEE*, and Jianping Yao, *Fellow, IEEE*

***Abstract*—A dual-passband microwave photonic filter (MPF) implemented based on phase-modulation to intensity-modulation (PM-IM) conversion using a phase modulator and an equivalent phase-shifted fiber Bragg grating (EPS-FBG) is proposed and experimentally demonstrated. The key component in the system is the EPS-FBG, which is designed and fabricated based on the equivalent phase-shift technique. The unique feature of the EPS-FBG is that equivalent phase shifts are introduced to both of the $\pm 1^{st}$ channels, leading to a notch in each of the two channels. Thus, by implementing PM-IM conversion in the two channels, two passbands are produced. The central frequency of each passband is determined by the wavelength different between the notch and the optical carrier. In the design and fabrication, two phase shifts are introduced to the EPS-FBG to decrease the shape factor, which is defined as the ratio between the 20- and 3-dB bandwidths. In addition, a stimulated Brillouin scattering (SBS) assisted filter is incorporated in the system for carrier suppression to increase the spurious-free dynamic range (SFDR) and decrease the noise figure (NF) of the MPF. An experiment is performed. A dual passband filter with a 3-dB bandwidth and a shape factor of 167.3 MHz and 3.8, and 143.3 MHz and 3.3 for the 1^{st} and 2^{nd} passband is achieved. The frequency tunable ranges of the 1^{st} and 2^{nd} passbands are 5.4 and 7.4 GHz, respectively, with the magnitude variations of about ± 0.5 dB during the turning. Due to the SBS-assisted filter, the SFDRs are increased by 7 dB and the NFs are decreased by 10 dB.**

***Index Terms*—Dual passband, equivalent phase shift (EPS), fiber Bragg grating (FBG), microwave photonic filter (MPF).**

I. Introduction

OVER THE past few decades, microwave filters with dual passbands have attracted great interests due to the increasing demand for multiband/multifunctional microwave systems that support various modern services. Such systems require microwave circuits and components that can handle several different frequency bands [1]–[3]. Various dual-passband microwave filters have been reported recently. A dual-passband microwave filter can be implemented using two resonators, such as stepped-impedance resonators, stub-loaded open-loop resonators, and E-shaped resonators [4]–[6]. A dual-passband microwave filter can also be achieved by using a single resonator, such as a ring resonator, a patch resonator, and a quadruple-mode resonator [7]–[9]. However, most of the dual-passband microwave filters have two fixed passbands. Recently, a dual-passband microwave filter with two tunable passbands is proposed for selectable multimode or multiband applications that have different operating frequencies [10], [11]. However, the frequency tunable range is only about 0.5 GHz. On the other hand, microwave filters implemented based on photonics have been extensively researched in the last 20 years because of their advantageous features, such as high frequency and large frequency tunable range [12], [13]. A microwave photonic filter (MPF) can be realized based on a delay-line structure with a finite impulse response (FIR) [14]–[16]. Due to the discrete number of taps, the spectral response is periodic with multiple passbands. To achieve an MPF with a single passband, one simple solution is to use stimulated Brillouin scattering (SBS) in which the Brillouin gain is employed to selectively amplify the sideband of a single-sideband modulated optical signal [17]. Recently, a simpler approach to achieving a single passband MPF was reported in which a phase-modulated optical signal is converted to an intensity-modulated signal by suppressing one sideband and amplifying the other sideband based on the SBS effect using a dual-sideband suppressed-carrier pump [18]. A single-passband MPF can also be obtained using an optical filter to suppress one of the sidebands of a phase-modulated signal. The optical filters include two cascaded fiber Bragg gratings (FBGs), a ring resonator, or a phase-shifted fiber Bragg grating (PS-FBG) [19]–[22]. Due to the wide bandwidth of a ring resonator, an MPF based on a ring resonator has a wide passband, which is in the range of several gigahertz [21]. On the other hand, by using a PS-FBG, an MPF with a much narrower passband can be achieved [22]. The MPFs proposed above have a single passband or multiple periodic passbands, and they cannot be used for applications where two independently tunable passbands are needed.

In this paper, we propose and experimentally demonstrate, for the first time to the best of our knowledge, an MPF with two

Manuscript received June 29, 2013; revised November 21, 2013; accepted November 22, 2013. Date of publication January 02, 2014; date of current version February 03, 2014. The work of L. Gao was supported in part by the China Scholarship Council under a scholarship. This work was supported by the Natural Science and Engineering Research Council of Canada (NSERC).

L. Gao is with the Microwave Photonics Research Laboratory, School of Electrical Engineering and Computer Science, University of Ottawa, ON K1N 6N5, Canada, and also with the National Laboratory of Solid State Microstructures and College of Engineering and Applied Sciences, Nanjing University, Nanjing 210093, China.

J. Zhang and J. Yao are with the Microwave Photonics Research Laboratory, School of Electrical Engineering and Computer Science, University of Ottawa, ON K1N 6N5, Canada (e-mail: jpyao@eecs.uottawa.ca).

X. Chen is with the National Laboratory of Solid State Microstructures and College of Engineering and Applied Sciences, Nanjing University, Nanjing 210093, China.

Color versions of one or more of the figures in this paper are available online at http://ieeexplore.ieee.org.

Digital Object Identifier 10.1109/TMTT.2013.2294601

independently tunable passbands based on phase-modulation to intensity-modulation (PM-IM) conversion using a phase modulator (PM) and an equivalent phase-shifted fiber Bragg grating (EPS-FBG). The key component in the proposed filter is the EPS-FBG, which is designed and fabricated by using the equivalent phase-shift technique [23]–[25]. The EPS-FBG has multiple channels due to the spatial sampling of the grating structure. Equivalent phase shifts introduced to the $\pm 1^{\text{st}}$ channels are realized through changing the sampling function. Therefore, the fabrication of an EPS-FBG is significantly simplified since the control of the spatial sampling is in a micrometer scale; while the control of the phase shift in the fabrication of a true PS-FBG is in a nanometer scale. In the design, two π phase shifts are introduced into both of the $\pm 1^{\text{st}}$ channels to produce an ultra-narrow and flat-bottom notch in each channel. A bandpass filter is achieved due to the PM-IM conversion by filtering one sideband of a phase-modulated signal. In the proposed approach, the PM-IM conversion is performed at the $\pm 1^{\text{st}}$ channels, thus two independently tunable passbands are generated. Since two π phase shifts are introduced to achieve flat-bottom notchs, the resulted passbands have small shape factors. Here, the shape factor is defined as the ratio between the 20- and 3-dB bandwidths. In addition, an SBS-assisted filter is employed to suppress the powers of the optical carriers, thus the spurious-free dynamic ranges (SFDRs) for the two passbands are increased and the noise figures (NFs) are reduced. In the experiment, the bandwidth and shape factor of the 1^{st} passband are 167.3 MHz and 3.8, and those of the 2^{nd} passband are 143.4 MHz and 3.3. The 1^{st} and 2^{nd} passband have frequency tunable ranges of 5.4 and 7.4 GHz, respectively. The variations of the magnitude over the tunable ranges are maintained within ± 0.5 dB. Due to the SBS-assisted filter, the SFDRs of the two passband filters are increased by 7 dB, and the NFs of the two passband filters are decreased by 10 dB.

II. Principle

The configuration of the proposed MPF is shown in Fig. 1. Two light waves generated from two tunable laser sources (TLSs) are sent to a PM via two polarization controllers (PCs) to align the polarization directions of the lightwaves with the principal axis of the PM. The PM is driven by a sinusoidal microwave signal with a tunable frequency generated by a vector network analyzer (VNA). The two phase-modulated signals are amplified by an erbium-doped fiber amplifier (EDFA1) and sent to an EPS-FBG via an optical circulator (OC1) for PM-IM conversion. One sideband of each of the phase-modulated signal is removed by the notch in each of the passbands. Thus, PM-IM conversion is implemented. The two single-sideband optical signals are then sent to a SBS-assisted filter to suppress the powers of the optical carriers. The SBS-assisted filter is implemented using two OCs, a section of dispersion-shifted fiber (DSF) and a PC (PC3). The signal at the output of the SBS-assisted filter is amplified by a second EDFA (EDFA2) and then detected at a photodetector (PD). The frequency response of the dual-passband filter is measured by feeding the detected signal to the VNA.

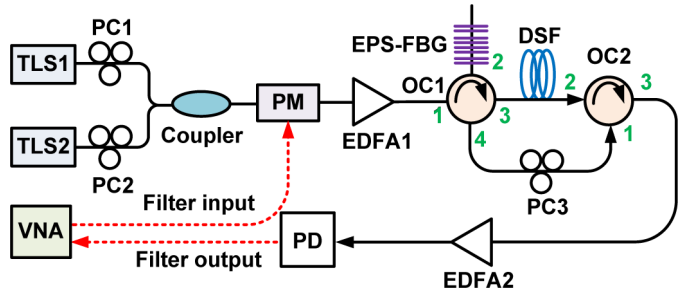

Fig. 1. Schematic of the proposed dual-passband MPF. Tunable laser source: TLS, polarization controller: PC, phase modulator: PM, erbium-doped fiber amplifier: EDFA, equivalent phase-shifted fiber Bragg grating: EPS-FBG, optical circulator: OC, dispersion-shifted fiber: DSF, photodetector: PD, vector network analyzer: VNA.

The key component in the dual-passband MPF is the EPS-FBG, which is realized through sampling to introduce equivalent π phase shifts to the $\pm 1^{\text{st}}$ channels. Mathematically, the index modulation of an EPS-FBG along the z-direction (axial direction) is given by [23]–[25]

$$\Delta n(z) = \begin{cases} \underbrace{\sum_m F_m \exp\left(j\frac{2\pi m}{P}z\right)}_{S(z)} \exp\left(j\frac{2\pi}{\Lambda}z\right) + c.c, & z \le z_k \\ \underbrace{\sum_m F_m \exp\left(j\frac{2\pi m}{P}(z+\Delta P)\right)}_{S(z+\Delta P)} \exp\left(j\frac{2\pi}{\Lambda}z\right) + c.c, & z > z_k \end{cases} \tag{1}$$

where Λ is the period of the grating, $S(z)$ is the spatial sampling function, F_m is the Fourier coefficient of the m^{th} channel, P is the sampling period of a uniform sampling function, and ΔP is the increase of sampling period at z_k. As can be seen, the amount of phase shift introduced to the m^{th} channel at z_k is given by

$$\theta_m = 2\pi m\left(\frac{\Delta P}{P}\right). \tag{2}$$

In the design, the $\pm 1^{\text{st}}$ channels are selected for their relatively large Fourier coefficient. According to (2), when ΔP is selected to be $P/2$, a π phase shift is introduced to the $\pm 1^{\text{st}}$ channels. Therefore, there is a notch in each of the $\pm 1^{\text{st}}$ channels. Note that by employing the sampling technique, in the fabrication of the EPS-FBG, only micrometer scale accuracy and a uniform phase mask is required. It is much simpler than the conventional method to achieve a PS-FBG where a true phase shift is introduced that requires nanometer scale accuracy or a PS phase mask with a high cost.

When the notch induced by a single π phase shift is employed to suppress one of the sidebands of a phase-modulated optical signal for PM-IM conversion, a Lorentz-shaped passband would be generated, and the shape factor of the filter is large [22]. The shape factor is a figure-of-merit that indicates the speed of the filter response falling from the passband to the stopband. A small shape factor indicates a good selectivity. To obtain a small shape factor, two π phase shifts are introduced to the EPS-FBG

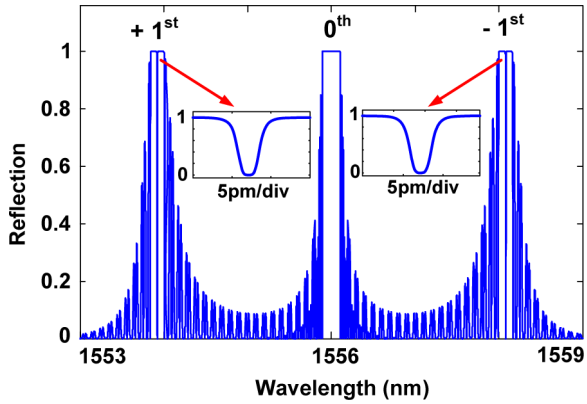

Fig. 2. Simulated reflection spectrum of an EPS-FBG with two phase shifts.

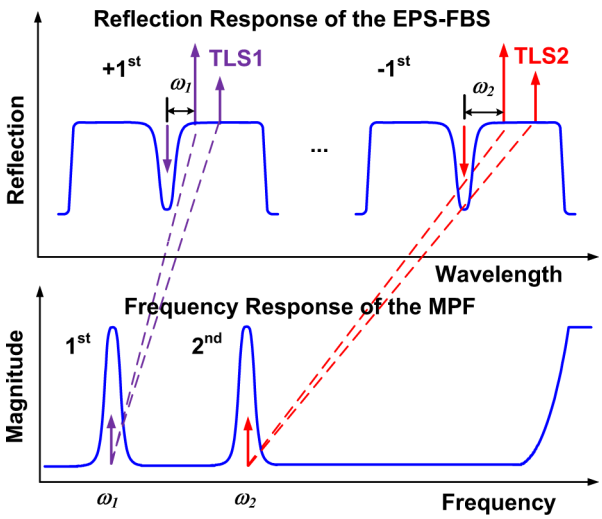

Fig. 3. Illustration of the generation of the two passbands.

to obtain two adjacent notches such that the overall notch has a relatively flat bottom [24]. The two π phase shifts are introduced at the $k/4^{\text{th}}$ and 3 $k/4^{\text{th}}$ periods, where k is the number of total sampling periods. The simulated reflection spectrum of an EPS-FBG with two π phase shifts is shown in Fig. 2. As can be seen, the notches are flatter than that of an EPS-FBG with only a single π phase shift [24].

The wavelengths of the optical carriers from TLS1 and TLS2 are tuned to locate at the $\pm 1^{\text{st}}$ channels of the EPS-FBG, as shown in Fig. 3. When one sideband of a phase-modulated signal is suppressed by the notch in the $+1^{\text{st}}$ channel, a passband with a central frequency of ω_1, the frequency difference between the optical carrier and the notch in $+1^{\text{st}}$ channel, will be produced due to the PM-IM conversion. Similarly, when one sideband of a phase-modulated signal is suppressed by the notch in the -1^{st} channel, a passband with a central frequency of ω_2, the frequency difference between the optical carrier and the notch in the -1^{st} channel, will also be produced. Therefore, there will be two passbands with the central frequencies of ω_1 and ω_2. The central frequencies of the passbands can be tuned by shifting the wavelengths of the TLSs independently.

The SBS-assisted filter in the system is employed to suppress the optical carriers [26]. When the lightwaves pass through the DSF, and the powers of the optical carriers are above the threshold of the SBS, Stokes waves are generated, which are

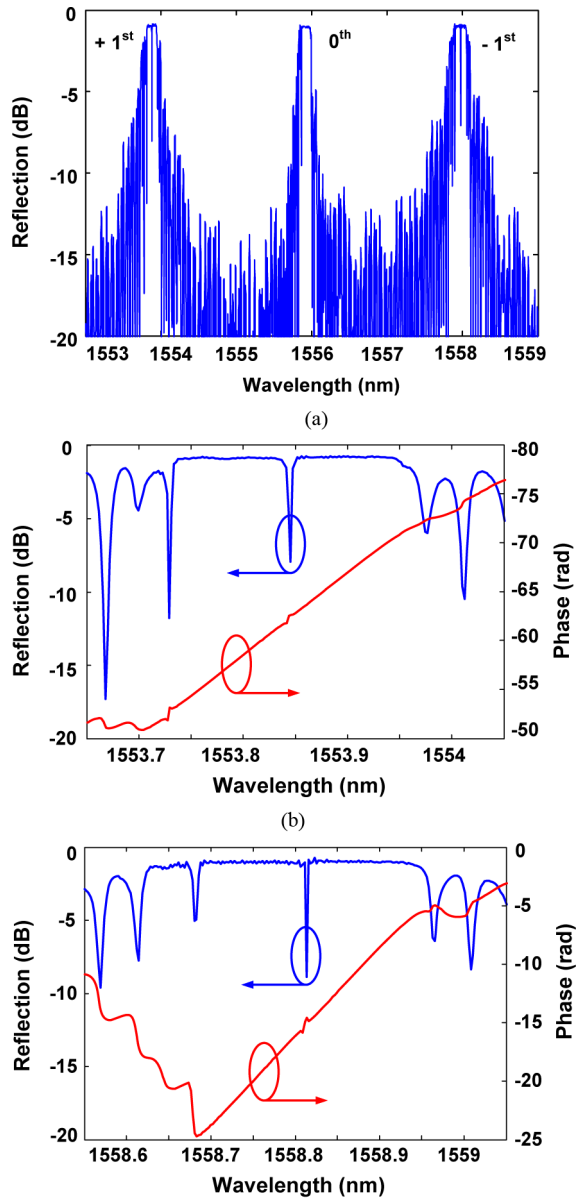

Fig. 4. (a) Measured reflection spectrum of the EPS-FBG. (b) Zoom-in view of the reflection spectrum and phase response of the $+1^{\text{st}}$ channel. (c) Zoom-in view of the reflection spectrum and phase response of the -1^{st} channel.

traveling along the DSF in an opposite direction of the optical carriers. Note that, under small-signal modulation condition, the powers of the sidebands are below the threshold of the SBS, thus SBS occurs only at the optical carriers and the sidebands are kept unchanged. The Stokes waves go through PC3, which is used to adjust the polarization state of the Stokes waves and then they are launched into the DSF via OC2. As the Stokes waves consecutively circulate in the ring, the optical carriers are suppressed. When the optical power at the input of the PD is constant, the suppression of the optical carriers will increase the gain of the system [27]. The SFDRs and NFs of the system are given as

$$\text{SFDR} = \frac{2}{3}\left(\text{IP}_3 - N_o + G\right) \tag{3a}$$

$$\text{NF} = \left[N_o - G - (-174)\right] \tag{3b}$$

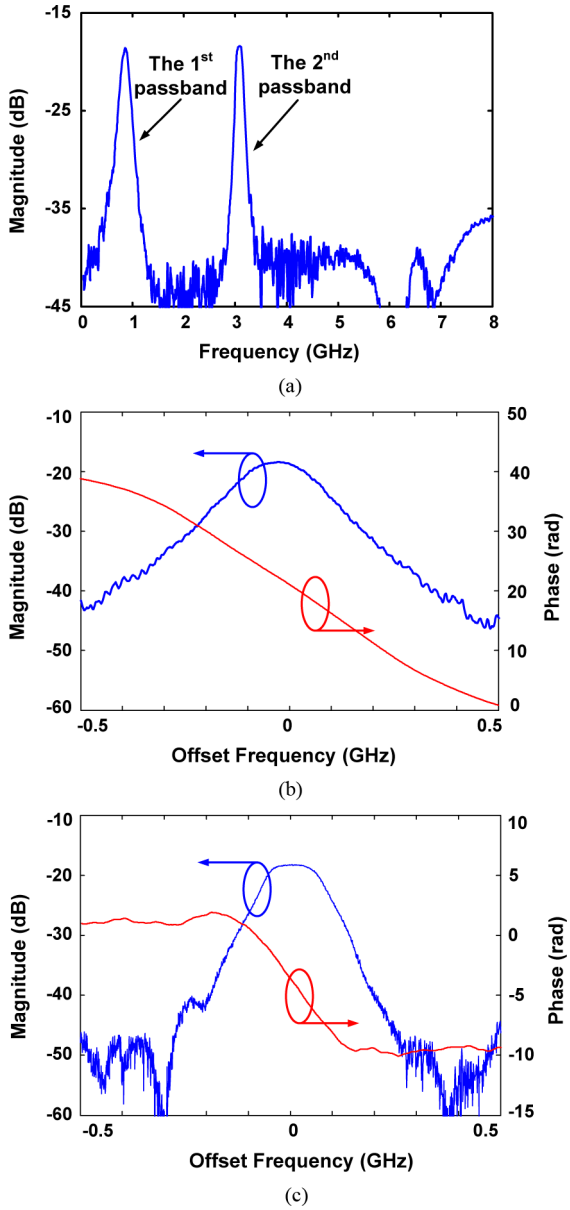

Fig. 5. (a) Frequency response of the dual-passband MPF. (b) Frequency response and phase response of the 1st passband. (c) Frequency response and phase response of the 2nd passband.

where IP_3 is the linearly extrapolated input power in dBm, where the fundamental and third-order intermodulation output powers would be equal, N_o is the value of the noise floor, G is the gain of the system, and the constant value of -174 dBm is the thermal noise power in a 1-Hz bandwidth at a noise temperature of 290 K. As shown in (3), an increase in the system gain will lead to an increase in the SFDRs and a decrease in the NFs simultaneously.

III. Experiment and Results

The EPS-FBG is fabricated by the equivalent phase-shift technique. The grating is imprinted into a hydrogen-loaded photosensitive fiber through a uniform phase masks by scanning a 244-nm UV beam from a frequency-doubled argon ion laser. The sampling structure of the EPS-FBG is calculated

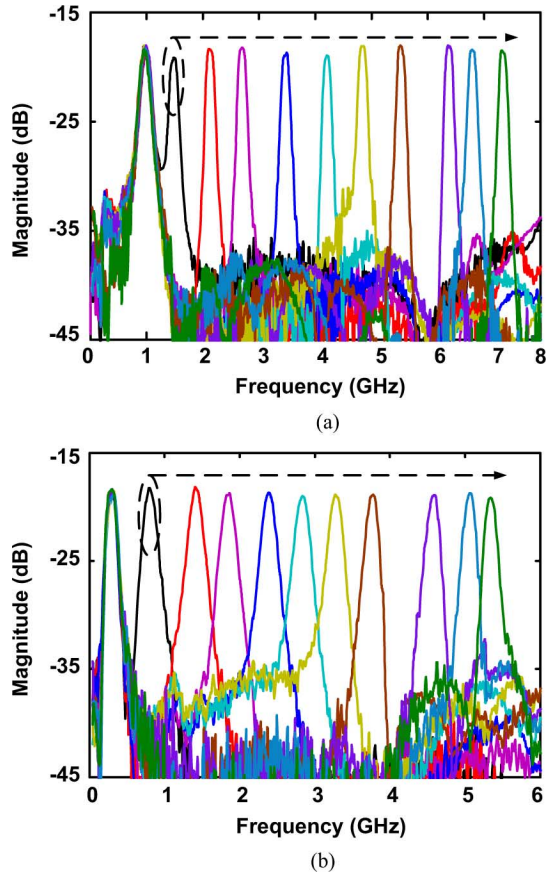

Fig. 6. (a) The 1st passband is kept unchanged, and the 2nd passband is tuned. (b) The 2nd passband is kept unchanged, and the 1st passband is tuned.

and loaded to a computer to control the movement of a translation stage and an optical shutter [25]. In the fabrication, the sampling period of the EPS-FBG is 0.4 mm, and there are totally 80 sampling periods. The phase shifts are introduced to the EPS-FBG by increasing the periods of the 20^{th} and 60^{th} samples by half the sampling period, which is 0.2 mm. The spectral response of the EPS-FBG is measured by an optical vector analyzer (OVA). As shown in Fig. 4(a), the EPS-FBG has multiple reflection bands due to the spatial sampling and there are phase shifts in both of the $\pm 1^{\text{st}}$ channels. The zoom-in views of the $\pm 1^{\text{st}}$ channels are given in Fig. 4(b) and (c). The bandwidths of the $\pm 1^{\text{st}}$ and -1^{st} channels are about 24 and 30 GHz, respectively. The bandwidth difference between the $\pm 1^{\text{st}}$ channels is mainly caused by the asymmetry during the fabrication process. The reflection bandwidths and notch bandwidths of the $\pm 1^{\text{st}}$ channels can be controlled through changing the maximum modulation index and the length of the EPS-FBG [24].

The fabricated EPS-FBG is then incorporated in the MPF system, as shown in Fig. 1. Two lightwaves from two TLSs (Anritsu MG9638A, and Yokogawa AQ2201) both with the powers of 5 dBm are sent to the PM (JDSU, 20 GHz) via their respective PCs (PC1 and PC2). A microwave signal from a VNA (Agilent E8364A, 50 GHz) is applied to the PM via the RF port. The phase-modulated signals are sent to the EPS-FBG via OC1 after amplified by EDFA1, and the output power from EDFA1 is 15 dBm. The optical signals reflected from the EPS-FBG are

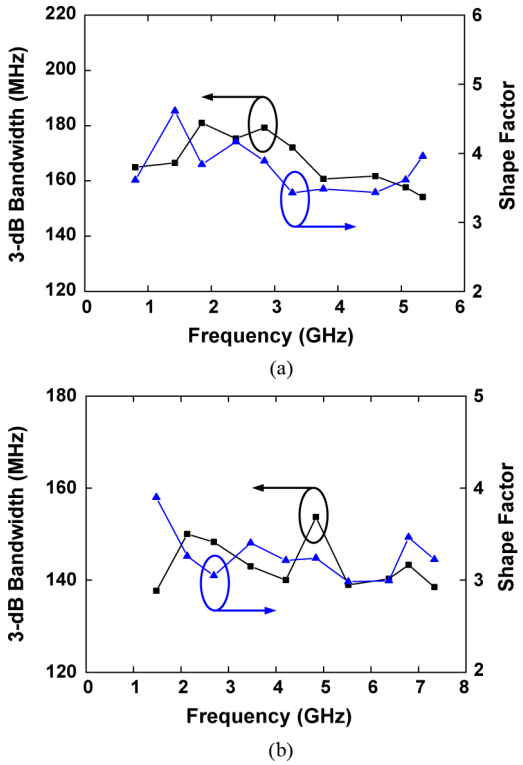

Fig. 7. The 3-dB bandwidth and the shape factor of the: (a) 1^{st} passband and (b) 2^{nd} passband at different frequencies.

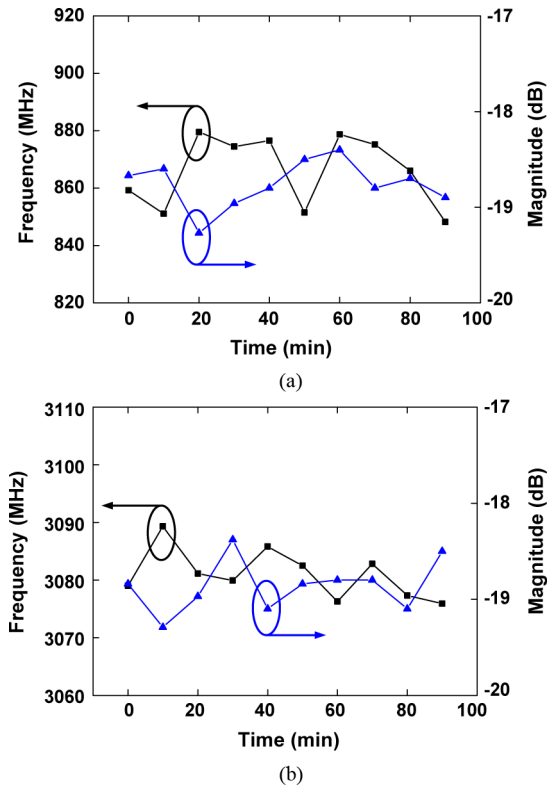

Fig. 8. Frequency and magnitude variations of the: (a) 1^{st} passband and (b) 2^{nd} passband in 1.5 h. The measurements are taken with a 10-min interval.

then routed by OC1 to an SBS-assisted filter for optical carrier suppression. The SBS-assisted filter includes two OCs (OC1 and OC2), a section of DSF of 9 km, and a PC (PC3). After the optical signals are amplified by EDFA2 with an output power of 0 dBm, they are sent to the PD (Nortel Networks, 3-dB bandwidth of 10 GHz, and responsivity of 0.83 A/ W) for optical-to-electrical conversion. The generated electrical signal from the PD is sent back to the VNA for frequency response measurement. The wavelengths of optical carriers from the TLSs are controlled to be at the $\pm 1^{st}$ channels, respectively. The PM-IM conversion is realized at the $\pm 1^{st}$ channels by using the respective notches to suppress one of the respective sidebands. Thus, two passbands are produced, as shown in Fig. 5(a). The zoom-in views of the two passbands are given in Fig. 5(b) and (c). The 1^{st} passband obtained by the PM-IM conversion in the $+1^{st}$ channel has a 3-dB bandwidth of 165 MHz and a shape factor of 4.1. The 2^{nd} passband achieved by the PM-IM conversion in the -1^{st} channel has a 3-dB bandwidth of 143 MHz and a shape factor of 2.9. Linear phase responses are achieved in the two passbands, as also shown in Fig. 5(b) and (c). The insertion loss of the MPF is 18.7 dB.

The frequency tunability of the MPF is then investigated. Firstly, the 1^{st} passband with a central frequency of about 1 GHz is kept unchanged, and the 2^{nd} passband is tuned. As can be seen, the central frequency of the 2^{nd} passband is shifted from 1.5 to 7.4 GHz, realized by tuning the wavelength of the TLS2, as shown in Fig. 6(a). The 2^{nd} passband with a central frequency of about 0.2 GHz is then kept unchanged, and the 1^{st} passband is tuned. As can be seen, the central frequency of the 1^{st} passband is shifted from 0.8 to 5.4 GHz, realized by tuning the wavelength of TLS1, as shown in Fig. 6(b). As can be seen, there are small magnitude variations during the frequency tuning, which are about ± 0.5 dB.

The 3-dB bandwidths and shape factors of the two passbands at different frequencies are also measured and given in Fig. 7. As can be seen, the average 3-dB bandwidth of the 1^{st} passband is 167.3 MHz, and the variations are within ± 13 MHz. The average shape factor is 3.8, and the variations are within ± 0.3. The average 3-dB bandwidth of the 2^{nd} passband is 143.4 MHz, and the variations are within ± 7 MHz. The average shape factor is 3.3, and the variations are within ± 0.3 . Since there are two phase shifts in each of the $\pm 1^{st}$ channels, the shape factors are decreased significantly compared with the use of a PS-FBG with only a single π phase shift, as reported in [22], in which the shape factors are 7.5 and 10. In addition, the small magnitude and bandwidth variations at different frequencies are important for applications where the loss or bandwidth is required to be constant.

The stability of the MPF is also studied. To do so, the MPF is allowed to operate at room temperature for 1.5 h. Fig. 8 shows the central frequencies and magnitudes of the two passbands measured with a 10-min interval. The frequency and magnitude variations of the 1^{st} passband are within ± 16 MHz and ± 0.5 dB, respectively. The frequency and magnitude variations of the 2^{nd} passband are within ± 9 MHz and ± 0.5 dB, respectively. The frequency stability of the MPF depends mainly on the wavelength stability of the TLSs and the EPS-FBG. To have

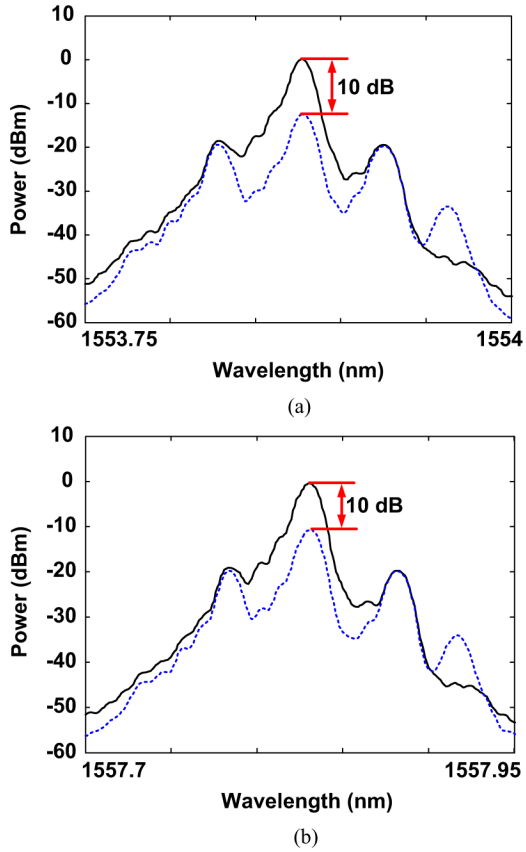

Fig. 9. Optical spectrum of the: (a) 1st phase-modulated signal and (b) 2nd phase-modulated signal without (black-solid line) and with (blue-dashed line) the SBS-assisted filter.

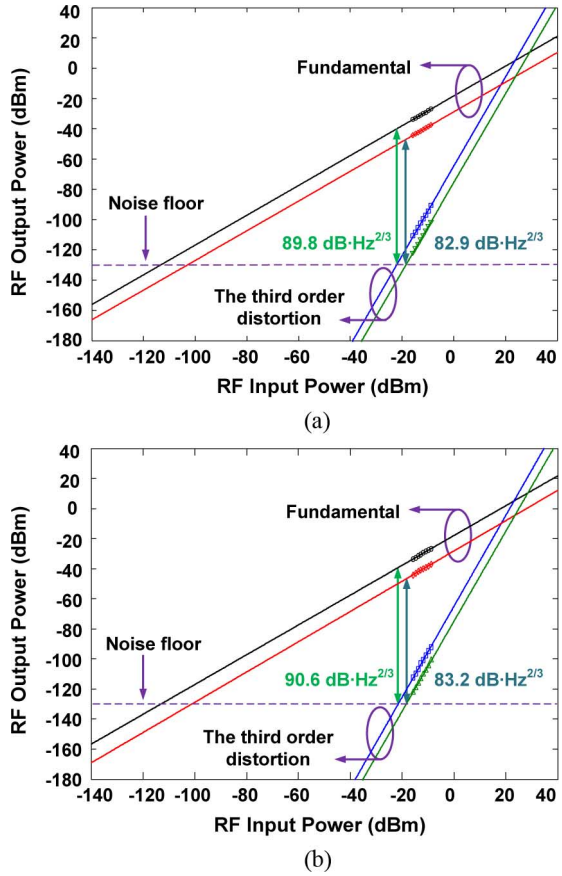

Fig. 10. Measured fundamental output power and third-order distortion power for the: (a) 1st passband and (b) 2nd passband without and with the SBS-assisted filter.

a better frequency stability, TLSs with better wavelength stability should be used. In addition, the EPS-FBG should be well packaged with temperature control such that the effect of the environment disturbance on the stability will be significantly reduced.

The performance improvement due to the incorporation of the SBS-assisted filter is also studied. To do so, we measure the optical spectrums and the SFDRs of the dual-passband MPF without and with the SBS-assisted filter. We first disconnect PC3 with port 1 of OC2, thus the SBS-assisted filter is no longer operating in the MPF. The optical spectrums of the two phase-modulated signals are shown in Fig. 9(a) and (b). PC3 is then connected with port 1 of OC2, and the SBS-assisted filter starts operating in the MPF. The Stokes waves consecutively circulate in the ring and the optical carriers are greatly suppressed. The optical spectrums of the two phase-modulated signals are also shown in Fig. 9(a) and (b). As can be seen from Fig. 9, the optical carriers are both suppressed by about 10 dB. The sidebands are almost unchanged since the powers of the sidebands are kept below the threshold of the SBS in the experiment, and no SBS effects are produced for the sidebands.

The SFDRs of the MPF for the two passbands are measured and given in Fig. 10. The measured SFDRs of the 1st and 2nd passbands are 82.9 dB $\cdot$ Hz$^{2/3}$ and 83.2 dB $\cdot$ Hz$^{2/3}$, respectively, when the SBS-assisted filter is not incorporated in the system. After connecting PC3 with port 1 of OC2, the optical carriers are suppressed greatly, and when the optical power at the input of the PD is kept the same as that without carrier suppression, the gain of the system is improved by about 10 dB. The measured SFDRs of the 1st and 2nd passbands are then 89.8 dB $\cdot$ Hz$^{2/3}$ and 90.6 dB $\cdot$ Hz$^{2/3}$, respectively, which are improved by about 7 dB.

According to (3b), the NFs will also be decreased by 10 dB from 72 to 62 dB. Note that, in the experiment, the noise floor is -130 dBm/Hz, restricted by the EDFAs and the TLSs used in the experiment. If the EDFAs are removed from the system, and TLSs with narrower linewidths and higher powers are used, a lower noise floor can be achieved [28], [29]. Thus, the SFDRs will be increased and the NFs will be reduced.

IV. Conclusion

An MPF with two independently tunable passbands was proposed and experimentally demonstrated based on PM-IM conversion using a PM and an EPS-FBG. The key component in the proposed MPF was the EPS-FBG, which was designed and fabricated based on the equivalent phase-shift technique through spatial sampling. Two phase shifts were introduced to the EPS-FBG to decrease the shape factors. Through PM-IM conversion, an MPF with two passbands was achieved. The two passband of the MPF could be tuned independently. In the experiment, the frequency tunable ranges of the two passbands were measured to be 5.4 and 7.4 GHz. The magnitude responses, bandwidths, and shape factors during the tuning were

maintained almost unchanged. To improve the performance of the MPF including increasing the SFDRs and reducing the NFs, an approach to suppressing the optical carriers by incorporating an SBS-assisted filter was employed. In the experiment, the SFDRs were increased by 7 dB, and the NFs were decreased by 10 dB thanks to the use of the SBS-assisted filter. The stability of the MPF was also studied. Under room temperature, the frequency and magnitude variations of the 1^{st} passband and 2^{nd} passband in 1.5 h were within $\pm$16 MHz, $\pm$0.5 dB, $\pm$9 MHz, and $\pm$0.5 dB, respectively.

REFERENCES

[1] J. Lee, M. S. Uhm, and I. B. Yom, "A dual-passband filter of canonical structure for satellite applications," *IEEE Microw. Wireless Compon. Lett.*, vol. 14, no. 6, pp. 271–273, Jun. 2004.

[2] G. Macchiarella and S. Tamiazzo, "Design techniques for dual-passband filters," *IEEE Trans. Microw. Theory Techn.*, vol. 53, no. 11, pp. 3265–3271, Nov. 2005.

[3] W. C. Chang and C. Y. Chang, "Analytical design of microstrip short-circuit terminated stepped-impedance resonator dual-band filters," *IEEE Trans. Microw. Theory Techn.*, vol. 59, no. 7, pp. 1730–1739, Jul. 2011.

[4] Y. P. Zhang and M. Sun, "Dual-band microstrip bandpass filter using stepped-impedance resonators with new coupling schemes," *IEEE Trans. Microw. Theory Techn.*, vol. 54, no. 10, pp. 3779–3785, Oct. 2006.

[5] P. Mondal and M. K. Mondal, "Design of dual-band bandpass filters using stub-loaded open-loop resonators," *IEEE Trans. Microw. Theory Techn.*, vol. 56, no. 1, pp. 150–154, Jan. 2008.

[6] Y. T. Kuo and C. Y. Chang, "Analytical design of two-mode dual-band filters using E-shaped resonators," *IEEE Trans. Microw. Theory Techn.*, vol. 60, no. 2, pp. 250–260, Feb. 2012.

[7] S. Sun, "A dual-band bandpass filter using a single dual-mode ring resonator," *IEEE Microw. Wireless Compon. Lett.*, vol. 21, no. 6, pp. 298–300, Jun. 2011.

[8] R. Zhang, L. Zhu, and S. Luo, "Dual-mode dual-band bandpass filter using a single slotted circular patch resonator," *IEEE Microw. Wireless Compon. Lett.*, vol. 22, no. 5, pp. 233–235, May 2012.

[9] J. Xu, W. Wu, and C. Miao, "Compact and sharp skirts microstrip dual-mode dual-band bandpass filter using a single quadruple-mode resonator (QMR)," *IEEE Trans. Microw. Theory Techn.*, vol. 61, no. 3, pp. 1104–1113, Mar. 2013.

[10] G. Chaudhary, Y. Jeong, and J. Lim, "Harmonic suppressed dual-band-bandpass filters with tunable passbands," *IEEE Trans. Microw. Theory Techn.*, vol. 60, no. 7, pp. 2115–2123, Jul. 2012.

[11] G. Chaudhary, Y. Jeong, and J. Lim, "Dual-band bandpass filter with independently tunable center frequencies and bandwidths," *IEEE Trans. Microw. Theory Techn.*, vol. 61, no. 1, pp. 107–116, Jan. 2013.

[12] J. P. Yao, "Microwave photonics," *J. Lightw. Technol.*, vol. 27, no. 2, pp. 314–335, Feb. 2009.

[13] J. Capmany, B. Ortega, and D. Pastor, "A tutorial on microwave photonic filters," *J. Lightw. Technol.*, vol. 24, no. 1, pp. 201–229, Jan. 2006.

[14] D. Pastor, B. Ortega, J. Capmany, S. Sales, A. Martinez, and P. Muñoz, "Optical microwave filter based on spectral slicing by use of arrayed waveguide gratings," *Opt. Lett.*, vol. 28, no. 19, pp. 1802–1804, Oct. 2003.

[15] B. Vidal, T. Mengual, C. Ibanez-Lopez, and J. Marti, "WDM photonic microwave filter with variable cosine windowing based on a DGD module," *IEEE Photon. Technol. Lett.*, vol. 18, no. 21, pp. 2272–2274, Nov. 2006.

[16] J. Mora, B. Ortega, A. Diez, J. L. Cruz, M. V. Andres, J. Capmany, and D. Pastor, "Photonic microwave tunable single-bandpass filter based on a Mach–Zehnder interferometer," *J. Lightw. Technol.*, vol. 24, no. 7, pp. 2550–2509, Jul. 2006.

[17] B. Vidal, M. A. Piqueras, and J. Martí, "Tunable and reconfigurable photonic microwave filter based on stimulated Brillouin scattering," *Opt. Lett.*, vol. 32, no. 1, pp. 23–24, Jan. 2007.

[18] W. Zhang and R. A. Minasian, "Widely tunable single-passband microwave photonic filter based on stimulated Brillouin scattering," *IEEE Photon. Technol. Lett.*, vol. 23, no. 23, pp. 1775–1777, Dec. 2011.

[19] X. Yi and R. A. Minasian, "Microwave photonic filter with single bandpass response," *Electron. Lett.*, vol. 45, no. 7, pp. 362–363, Mar. 2009.

[20] T. Chen, X. Yi, L. Li, and R. Minasian, "Single passband microwave photonic filter with wideband tunability and adjustable bandwidth," *Opt. Lett.*, vol. 37, no. 22, pp. 4699–4701, Nov. 2012.

[21] J. Palací, G. E. Villanueva, J. V. Galán, J. Martí, and B. Vidal, "Single bandpass photonic microwave filter based on a notch ring resonator," *IEEE Photon. Technol. Lett.*, vol. 22, no. 17, pp. 1276–1278, Sep. 2010.

[22] W. Li, M. Li, and J. P. Yao, "A narrow-passband and frequency-tunable micro-wave photonic filter based on phase-modulation to intensity-modulation conversion using a phase-shifted fiber Bragg grating," *IEEE Trans. Microw. Theory Techn.*, vol. 60, no. 5, pp. 1287–1296, May 2012.

[23] Y. Dai, X. Chen, D. Jiang, S. Xie, and C. Fan, "Equivalent phase shift in a fiber Bragg grating achieved by changing the sampling period," *IEEE Photon. Technol. Lett.*, vol. 16, no. 10, pp. 2284–2286, Oct. 2004.

[24] L. Gao, X. Chen, and J. P. Yao, "Tunable microwave photonic filter with a narrow and flat-top passband," *IEEE Microw. Wireless Compon. Lett.*, vol. 23, no. 7, pp. 362–364, Jul. 2013.

[25] L. Gao, X. Chen, J. Xiong, S. Liu, and T. Pu, "Fabricating fiber Bragg gratings with two phase masks based on reconstruction-equivalent-chirp technique," *Opt. Exp.*, vol. 20, no. 3, pp. 2240–2245, Jan. 2012.

[26] B. Chen, S. Zheng, H. Chi, X. Zhang, and X. Jin, "An optical millimeter- wave generation technique based on phase modulation and Brillouin-assisted notch-filtering," *IEEE Photon. Technol. Lett.*, vol. 20, no. 24, pp. 2057–2059, Dec. 2008.

[27] L. Liu, S. Zheng, X. Zhang, X. Jin, and H. Chi, "Performances improvement in radio over fiber link through carrier suppression using stimulated Brillouin scattering," *Opt. Exp.*, vol. 18, no. 11, pp. 11 827–11 837, May 2010.

[28] D. Marpaung, C. Roeloffzen, A. Leinse, and M. Hoekman, "A photonic chip based frequency discriminator for a high performance microwave photonic link," *Opt. Exp.*, vol. 18, no. 26, pp. 27 359–27 370, 2010.

[29] M. Huang, J. Fu, and S. Pan, "Linearized analog photonic links based on a dual-parallel polarization modulator," *Opt. Lett.*, vol. 37, no. 11, pp. 1823–1825, Jun. 2012.

Liang Gao (S'12) received the B.S. degree from the College of Engineering and Applied Sciences, Nanjing University, Nanjing, China, in 2009, and is currently working toward the Ph.D. degree under a joint program in the College of Engineering and Applied Sciences, Nanjing University, Nanjing, China, and the Microwave Photonics Research Laboratory, School of Electrical Engineering and Computer Science, University of Ottawa, Ottawa, ON, Canada.

His research interests include fiber-optic sensors, microwave photonics, fiber Bragg gratings (FBGs), and optical communications.

Jiejun Zhang (S'12) received the B.S. degree in electronic science and technology from the Harbin Institute of Technology, Harbin, China, in 2010, the M.S. degree in optical engineering from the Huazhong University of Science and Technology, Huazhong, China, in 2013, and is currently working toward the Ph.D. degree at the University of Ottawa, Ottawa, ON, Canada.

He is currently with the Microwave Photonics Research Laboratory, School of Electrical Engineering and Computer Science, University of Ottawa. His research interests include fiber-optic sensors and microwave waveform generation based on fiber-optic systems.

Xiangfei Chen (M'05–SM'12) received the Ph.D. degree in physics from Nanjing University, Nanjing, China, in 1996.

From 1996 to 2000, he was a faculty member with the Nanjing University of Post and Telecommunication Technology, where he has been engaged in the research and development of fiber optic components. From 2000 to 2006, he was an Associate Professor with the Department of Electrical Engineering, Tsinghua University, Beijing, China, where he was engaged in the research and development of novel FBG based devices and their applications in fiber-optic system. From October 2004 to April 2005, he was a Visiting Scholar with the Microwave Photonics Research Laboratory, School of Information Technology and Engineering, University of Ottawa, Ottawa, ON, Canada. He is currently a Professor with the Microwave Photonics Technology Laboratory, National Laboratory of Solid State Microstructures and College of Engineering and Applied Sciences, Nanjing University, Nanjing, China. He has authored or coauthored more than 120 international technical papers and conference papers. He also holds a number of patents. His current research has focused on the development of photonic integration circuits, novel fiber-optic devices for high-speed large-capacity optical networks, microwave photonics, and fiber-optic sensors.

Dr. Chen is a Senior Member of the IEEE Photonics Society and the IEEE Microwave Theory and Techniques Society (IEEE MTT-S). He is a member of the Optical Society of American (OSA).

Jianping Yao (M'99–SM'01–F'12) received the Ph.D. degree in electrical engineering from the Université de Toulon, Toulon, France, in 1997.

In 2001, he joined the School of Electrical Engineering and Computer Science, University of Ottawa, Ottawa, ON, Canada, as an Assistant Professor, and became an Associate Professor in 2003 and a Full Professor in 2006. In 2007, he was appointed University Research Chair in Microwave Photonics. From July 2007 to June 2010, he was Director of the Ottawa–Carleton Institute for Electrical and Computer Engineering. Prior to joining the University of Ottawa, from 1999 to 2001, he was an Assistant Professor with the School of Electrical and Electronic Engineering, Nanyang Technological University, Singapore. He has authored or coauthored over 420 papers, including more than 240 papers in peer-reviewed journals and 180 papers in conference proceedings.

Dr. Yao is a Registered Professional Engineer in the Province of Ontario. He is a Fellow of Optical Society of America (OSA) and the Canadian Academy of Engineering. He has been a chair of numerous international conferences, symposia, and workshops including the vice Technical Program Committee (TPC) chair of the 2007 IEEE Microwave Photonics Conference, TPC co-chair of the 2009 and 2010 Asia–Pacific Microwave Photonics Conferences, TPC chair of the High-Speed and Broadband Wireless Technologies Subcommittee of the 2009–2012 IEEE Radio Wireless Symposia, TPC chair of the Microwave Photonics Subcommittee of the 2009 IEEE Photonics Society Annual Meeting, TPC chair of the 2010 IEEE Microwave Photonics Conference, and general co-chair of the 2011 IEEE Microwave Photonics Conference. He was the recipient of the 2005 International Creative Research Award of the University of Ottawa, and the 2007 George S. Glinski Award for Excellence in Research. He was also the recipient of an inaugural OSA Outstanding Reviewer Award in 2012. He is an IEEE Distinguished Microwave Lecturer (2013–2015).